Journal of Systems Engineering and Electronics
Vol. 35, No. 3, June 2024, pp.666 – 678

A deep multimodal fusion and multitasking trajectory prediction model for typhoon trajectory prediction to reduce flight scheduling cancellation

TANG Jun*, QIN Wanting, PAN Qingtao, and LAO Songyang

College of Systems Engineering, National University of Defense Technology, Changsha 410000, China

Abstract: Natural events have had a significant impact on overall flight activity, and the aviation industry plays a vital role in helping society cope with the impact of these events. As one of the most impactful weather typhoon seasons appears and continues, airlines operating in threatened areas and passengers having travel plans during this time period will pay close attention to the development of tropical storms. This paper proposes a deep multimodal fusion and multitasking trajectory prediction model that can improve the reliability of typhoon trajectory prediction and reduce the quantity of flight scheduling cancellation. The deep multimodal fusion module is formed by deep fusion of the feature output by multiple submodal fusion modules, and the multitask generation module uses longitude and latitude as two related tasks for simultaneous prediction. With more dependable data accuracy, problems can be analysed rapidly and more efficiently, enabling better decision-making with a proactive versus reactive posture. When multiple modalities coexist, features can be extracted from them simultaneously to supplement each other's information. An actual case study, the typhoon Lichma that swept China in 2019, has demonstrated that the algorithm can effectively reduce the number of unnecessary flight cancellations compared to existing flight scheduling and assist the new generation of flight scheduling systems under extreme weather.

Keywords: flight scheduling optimization, deep multimodal fusion, multitasking trajectory prediction, typhoon weather, flight cancellation, prediction reliability.

DOI: 10.23919/JSEE.2024.000042

1. Introduction

With the development of the present era, one positive point is that each new generation of aircraft shrinks the globe by decreasing the flying time between districts [1]. More people than ever before are flying, using air flight as a standard mode of transportation much like the automobile. Air travel faces myriad operational challenges: schedule disruptions, limited resources such as aircraft, crew and maintenance personnel, and increasing customer expectations. Irregular operations that occur, from as simple an event as a mechanical problem on a single aircraft to more impactful events such as a weather typhoon, can close many airports and cancel numerous flights. Typhoons usually refer to tropical cyclones that occur in the Northwest Pacific and South China Sea; tropical cyclones in the Indian Ocean, Arabian Sea and Bay of Bengal are often called cyclones; hurricanes generally refer to strong and deep tropical cyclones that occur in the Atlantic and eastern North Pacific. Typhoons, cyclones and hurricanes are all considered tropical cyclones that occur in the tropical ocean. Air travellers who experience extreme weather on trips know that it has a definite impact on air travel and its participants, airlines, ground handlers, airports and passengers [2].

Typhoons have caused significant concern and destruction across coastal countries and regions over the history of human development. Typhoons are one of the most severe weather events affecting human activities. With such a serious impact in the entire region, it is understandable that we need to be extra careful when travelling in traffic. Theoretically, if the height of a typhoon is not high, the plane can fly above it. Therefore, if the aircraft can fly above the typhoon and enter its sight, some people may feel that the airline can operate during the typhoon. However, this is not a common practice, as it may still be a risky move. Suppose there are any problems in the air; if surrounded by typhoons, that can have a huge impact [3,4]. For example, if there is a technical problem or an emergency medical situation, the crew will not have many options. The path of the typhoon may limit the pilot's solutions. Thus, because carriers want to avoid minor conflicts caused by typhoons, they must plan

Manuscript received May 17, 2022.
*Corresponding author.
This work was supported by the National Natural Science Foundation of China (62073330).

their operations ahead of time [5]. The overall track of the typhoon can be predicted several days in advance. Therefore, operators can make a prior decision on how to ensure the security of their services. Usually, if the typhoon approaches the neighbouring airport, they will cancel the flight and evacuate the aircraft as much as possible before arriving. In addition, flight travel exemptions are usually provided for passengers to and from affected cities. These factors would result in significant resource consumption and economic losses [6].

Perhaps with the continuous improvement of prediction and sensing technology, people may be more confident in conducting more routine flights at high altitudes or in typhoons. However, these cyclones often cause great damage across regions. Therefore, companies are more likely to choose avoidance as the best action plan. In general, similar to several other severe weather conditions, pilots can also minimize the risk of difficult situations in various ways. However, in harsh conditions, scientific and accurate predictions and planning are crucial to the decisions made by the crew when transporting passengers to their destinations. Typhoons and other extreme weather conditions can introduce problems ranging from increased turbulence, more difficult take-offs and landings, longer flights, more weight restrictions, airport closures, ground-related airport impacts and so on. The typical negative effects of flight cancellation decisions are as follows [7]:

(i) Irregular flight schedule;

(ii) Cost of passenger disruptions;

(iii) Customer loyalty decrease for the airline.

All airlines want to return to normal operations quickly to minimize the disruption and inconvenience caused to passengers. While many irregular operations, such as weather delays, are unavoidable, how an efficient airline responds to these disruptions is critical in maintaining passenger goodwill. The most salient limitation of current approaches is the lack of global situation awareness and precise prediction. The aim of this study is to optimize flight cancellations in adverse weather from an airport perspective in the joint airspace. We propose a deep multimodal fusion and multitasking trajectory prediction model that can improve the reliability of typhoon trajectory prediction and reduce the quantity of flight scheduling cancellation. With more dependable data accuracy, problems can be analysed rapidly and more efficiently, enabling better decision-making with a proactive versus reactive posture.

The organization of this paper is summarized as follows. In Section 2, we present an overview of flight scheduling optimization algorithms and state the problem of flight cancellation caused by typhoons. In Section 3, we discuss the proposed deep multimodal fusion and multitasking trajectory prediction model in detail. In Section 4, we illustrate the application of the methodology to a real typhoon case. Finally, Section 5 concludes this work and gives recommendations for future research.

2. Motivation and problem description

Weather prediction researchers are enhancing the quality of their weather forecasts, which are becoming more precise and granular in their data details. There have also been improvements in radar systems, light detection and ranging sensors and satellites, along with improved computer hardware performance, all improving weather predictions. In this paper, we mainly focus on the overview of flight scheduling optimization algorithms without discussing hardware improvements.

2.1 Overview of flight scheduling optimization algorithms

Table 1 shows the results of 20 references on flight scheduling in the last four years. Table 1 mainly introduces the model framework, key algorithms, model execution, model verification, and results publication time. For the model framework, it includes the stage division of the model, the number of targets and whether there is mathematical proof; the model execution is divided into two models, namely, static and real-time dynamic; for model verification, whether there is actual aviation data and whether it is compared with other models are tracked.

Table 1 Typical flight scheduling algorithms and respective characteristics in the last four years

Work	Model framework			Key algorithm	Model execution	Model verification		Year
	Stage	Target	Proof			Real data	Compared	
[8]	Four	Three	No	Mixed integer linear programming	Dynamic	French airspace	Yes	2020
[9]	Two	Single	No	Shift power law	Dynamic	Delta airlines	No	2019
[10]	Single	Three	Yes	Dantzig-Wolfe decomposition	Static	Iranian airlines	No	2018
[11]	Two	Two	No	Mixed integer linear programming	Static	Chinese airport	Yes	2020
[12]	Two	Two	No	Partheno-genetic algorithm	Static	No	Yes	2017

Continued

Work	Model framework			Key algorithm	Model execution	Model verification		Year
	Stage	Target	Proof			Real data	Compared	
[13]	Two	Single	No	Mixed integer linear programming	Static	No	Yes	2020
[14]	Three	Two	No	Genetic algorithm	Static	American airline	No	2017
[15]	Single	Single	No	Memetic algorithm	Static	Chinese airway network	Yes	2018
[16]	Two	Single	No	Sample average approximation	Static	Legacy airline company	Yes	2018
[17]	Single	Two	No	Genetic algorithm	Static	Chinese airspace	Yes	2018
[18]	Three	Three	Yes	Mixed integer nonlinear programming	Static	No	Yes	2018
[19]	Single	Single	Yes	Vertical navigation (VNAV) path model	Static	No	No	2017
[20]	Three	Single	No	Genetic algorithm	Dynamic	No	No	2019
[21]	Single	Single	Yes	Artificial bee colony algorithm	Static	No	Yes	2017
[22]	Single	Three	No	Simulated annealing algorithm	Static	Beijing-Tianjin-Hebei airport	Yes	2020
[23]	Single	Single	No	Mixed integer nonlinear programming	Static	Shanghai metroplex	Yes	2020
[24]	Single	Single	No	Max-plus model	Dynamic	No	No	2019
[25]	Single	Single	No	Network model	Static	Chinese airspace	No	2017
[26]	Two	Single	Yes	Particle swarm optimization	Static	Jeju international airport	Yes	2019
[27]	Two	Single	No	Integer linear programming	Static	Eastern China airline	Yes	2019

Specifically, Xu et al. [8] proposed a collaborative air traffic flow management framework within the scope of trajectory-based operations. The frame contains four modules. This modular design allows one or more modules to be flexibly adjusted for various purposes. The last model is abstracted into mixed integer linear programming, and the entire model is verified through actual cases in French airspace. Cao et al. [9] mainly explored the internal mechanism of flight departure delays from the perspective of mathematical statistics, and on this basis, from two aspects, namely, airport congestion and propagation delays, specific measures have been formulated to solve flight delays and further improve flight real-time scheduling performance. Finally, the verification of actual data from Delta airlines proves the effectiveness and practicability of the method. Khaksar et al. [10] compared the functions and economy of robust planning and interruption management under delayed conditions. The Dantzig-Wolfe decomposition method is used to solve this problem. The proposed technology is validated by major Iranian airlines. The calculation results show that this method can better solve the problem and greatly reduce flight delays. The main research purpose of [11] is to assign a group of flights to different runways, let each flight take off or land in turn, and determine their actual arrival and departure times. This paper proposes the improved partheno-genetic algorithm used in this research to simultaneously minimize flight delays and maximize runway utilization. To reduce the cost affected by ground services, Tang et al. [12] proposed a single genetic algorithm with hybrid heuristic rules to realize the coordination task scheduling plan among multiple services. At the same time, this paper also establishes a concurrent and chronological optimization model for multi-flight and multi-service problems. The test results show that the proposed model and algorithm are effective. Cecen et al. [13] proposed a random mixed integer linear programming model and used the simulated annealing algorithm to address aircraft scheduling. Then, the results of the stochastic method and the deterministic method are compared, showing that the stochastic version of the model can significantly reduce airborne delay. Because aircraft sequencing is flexible to changes in wind direction, the model can also easily find a new schedule for each aircraft. Abdelghany et al. [14] proposed a modelling framework for flight schedule planning that considers network-level competition with other airlines. This framework integrates genetic algorithms, network competition analysis models, and resource tracking models to form a random search technology. The model proposed in this paper is of great value to airline schedule planners. It can also be used to test long- and medium-term planning strategies. Wang et al. [15] proposed an improved memetic algorithm to solve the flight scheduling problem. The algorithm combines the local search with the global search strategy and uses the parallel memetic algorithm and the dynamic local search sampling strategy to control the number of local search samples. Experimental results show that the algorithm is robust and meets the requirements of time consistency. Kenan et al. [16] deve-

loped a two-stage stochastic planning model for flight scheduling and fleet allocation. The proposed model provides a solution that indicates which fleet will be allocated for each scheduled flight, considering the uncertainty of demand and ticket prices. The model is tested in real life, and sensitivity analysis is performed on some of the parameters. Xiao et al. [17] proposed a new hybrid indirect and direct coding genetic algorithm to solve the problem of air traffic network flow optimization. Experiments on comprehensive issues and actual data in China's airspace show that this method is superior to the direct coding method in terms of efficiency and effectiveness. Safak et al. [18] proposed a three-stage stochastic planning model that considers the randomness of demand and non-cruise time while determining the flight time, fleet allocation and aircraft routing issues. In numerical experiments, the method in this paper provides significant cost savings over two-stage stochastic programming and deterministic methods. In [19], a nominal flight time optimization strategy through the estimation/solution of delay accumulation was proposed. Through numerical traffic simulation, the feasibility of optimizing the nominal flight time is clearly proven. The main purpose of [20] is to provide intelligent decision support for the air traffic control automation system by accurately controlling the arrival time and flight profile of the aircraft. Specifically, this paper uses updated flight status data and scheduled arrival time to dynamically optimize the flight profile, continuously adjust the error of the aircraft arrival time, and realize four-dimensional trajectory guidance in real-time. The main goal of the study in [21] is to determine the optimal scheduling by evaluating the robustness of feasible solutions in their respective worst-case solutions. A new artificial bee colony algorithm is proposed and verified by experimental results. The algorithm can obtain near-optimal results with less computational cost within one hour of flight traffic planning. Geng et al. [22] established an optimized flight schedule model for a multi-airport integrated management system, including minimizing the maximum displacement of all flights, the weighted sum of total flight adjustments at each airport, and flight delays. An improved simulated annealing algorithm was designed to solve the proposed multiobjective optimization problem. Yang et al. [23] proposed formulas and solutions for a stochastic terminal flight arrival and departure scheduling problem under a performance based navigation environment. This paper provides an effective basis for complex mixed integer and nonlinear programming to solve this problem and demonstrates the capabilities of this method through test cases of actual terminal systems in the Shanghai metropolis. Han et al. [24] proposed a method for generating regular flights based on the max-plus model. First, a system model is established. Then, through the optimization algorithm, a conventional scheduling method is obtained. In this way, by combining system parameters and traffic flow data, the control method of the air traffic network can be pushed into, and the air traffic flow control strategy can adjust the large-scale airspace network in real-time. Zhao et al. [25] used the network model to transform the aircraft scheduling problem into a postman problem, which considers the connectivity of the airlines. This method considers not only the maximization of the company's interests but also the robustness of aircraft scheduling. To perform optimal and robust design in aircraft sequencing and scheduling problems, Hong et al. [26] proposed a two-stage stochastic programming algorithm based on particle swarm optimization. The decision-making problems in the first and second phases are defined as aircraft sequencing and scheduling, respectively, and the uncertainty generated by the flight time of the aircraft between two consecutive repairs is considered. Chen et al. [27] designed an air traffic control algorithm that can meet the airport throughput and flight service quality requirements in terms of flight delays. The algorithm expresses the flight scheduling problem via integer linear programming and then transforms it into a multiobjective optimization problem, which can be used to calculate the trade-off between scheduling resolution and time complexity. Based on multiobjective optimization, a heuristic algorithm considering time uncertainty is designed to improve airport throughput and reduce flight delay.

Based on the main content of the above 20 typical references, we can provide a further summary of the current research on flight scheduling problems. At present, to solve the related problems when designing a specific model, we can merge a variety of methods to form a multistage process for more effective and accurate solutions. The current commonly used model framework integrates mixed integer programming and swarm intelligence optimization algorithms to produce an effective and practical model. At the same time, as the model improves, more goals or factors can also be taken into consideration to form a comprehensive model that is closer to reality. However, we can also see that these current research methods also have certain shortcomings or can be further improved. Many models generally lack a theoretical proof process because it is very difficult to give a systematic derivation process. When testing the model in the early stage, most of the models do not pass the actual data test. Moreover, most of the current models do not have real-time and efficient computing capabilities and can only plan offline and static flights.

2.2 Flight cancellation caused by typhoons

These cyclones often cause great damage across regions, which can be harmful. Therefore, the highlights of flight scheduling optimization under typhoon weather are as follows:

(i) Monitor flight progress with forecast in advance;

(ii) Leverage previous weather content;

(iii) Proactively manage operations with intelligent alerting;

(iv) Help improve operational efficiency with smart methods;

(v) Streamline workflow to maintain airspace situation awareness.

As a typical case, the typhoon Lichma swept across China in 2019, causing a total of 14.024 million people in China and a direct economic loss of 53.72 billion Yuan [28]. Due to the typhoon, many airlines and airports cancelled some flights to ensure the safety of flight operations. We selected Beijing, Qingdao, Shanghai, Hangzhou, Guangzhou and Taipei from August 9th 2019 to August 11th 2019. The arrivals and cancellations of flights are shown in Table 2, and each day is divided into four time periods: 0:00-6:00, 6:00-12:00, 12:00-18:00, and 18:00-24:00. The data come from the Variflight App [29]. Therefore, mining the temporal and spatial patterns contained in the historical trajectory and predicting its position at a certain time in the future to achieve optimal flight scheduling through the predicted position have high application value. By reasonably predicting the typhoon trajectory, it is possible to maximize the optimization of flight scheduling and avoid the risks caused by improper flight scheduling. In Table 2, (x,y) represents the number of flights that arrive and are cancelled during the time period, where x represents the number of arriving flights, including the number of on-time arrivals and delayed arrivals, and y represents the number of cancelled flights, including the number of cancelled flights and alternate flights. Grey means that there are no flights in this time period; green means that all flights in this time period have arrived; yellow means that there are both arriving flights and cancelled flights in this time period; red means that all flights in this time period have been cancelled.

Table 2 Arrivals and cancellations of flights of Beijing, Qingdao, Shanghai, Hangzhou, Guangzhou and Taipei from August 9th 2019 to August 11th 2019

Start point	End point	August 9th				August 10th				August 11th			
		[0,6)	[6,12)	[12,18)	[18,24)	[0,6)	[6,12)	[12,18)	[18,24)	[0,6)	[6,12)	[12,18)	[18,24)
Beijing	Qingdao	(0,0)	(6,0)	(2,0)	(2,2)	(0,0)	(6,0)	(1,1)	(4,2)	(0,0)	(2,7)	(0,2)	(0,8)
	Shanghai	(0,0)	(17,1)	(3,15)	(0,14)	(0,0)	(0,18)	(1,22)	(0,13)	(0,0)	(17,3)	(18,2)	(11,3)
	Hangzhou	(1,0)	(11,0)	(2,4)	(0,8)	(0,1)	(2,9)	(1,7)	(4,4)	(1,0)	(11,1)	(5,1)	(9,0)
	Guangzhou	(0,0)	(13,0)	(13,1)	(4,3)	(0,0)	(9,4)	(13,0)	(7,0)	(0,0)	(12,1)	(13,0)	(7,0)
	Taipei	(0,0)	(2,2)	(1,0)	(1,0)	(0,0)	(2,0)	(2,0)	(1,0)	(0,0)	(2,0)	(1,0)	(2,0)
Qingdao	Beijing	(0,0)	(4,0)	(4,1)	(2,1)	(0,0)	(4,0)	(5,0)	(3,1)	(0,0)	(2,2)	(1,7)	(0,5)
	Shanghai	(0,0)	(8,1)	(6,3)	(0,10)	(0,0)	(0,11)	(0,9)	(0,9)	(0,0)	(6,5)	(2,7)	(2,7)
	Hangzhou	(0,0)	(3,0)	(3,1)	(0,1)	(0,0)	(0,4)	(0,4)	(0,2)	(0,0)	(2,1)	(1,3)	(0,1)
	Guangzhou	(0,0)	(3,0)	(4,0)	(4,0)	(0,0)	(3,0)	(4,0)	(3,2)	(0,0)	(3,0)	(1,3)	(0,5)
	Taipei	(0,0)	(0,1)	(0,2)	(0,0)	(0,0)	(0,0)	(1,0)	(0,0)	(0,0)	(0,0)	(1,0)	(0,0)
Shanghai	Beijing	(0,0)	(18,0)	(13,4)	(1,14)	(0,0)	(1,16)	(0,19)	(0,15)	(0,0)	(8,8)	(13,4)	(14,1)
	Qingdao	(0,0)	(9,2)	(7,1)	(0,11)	(0,0)	(0,11)	(0,8)	(0,10)	(0,0)	(0,12)	(3,4)	(3,7)
	Hangzhou	(0,0)	(0,0)	(0,0)	(0,0)	(0,0)	(0,0)	(0,0)	(0,0)	(0,0)	(0,0)	(0,0)	(0,0)
	Guangzhou	(0,0)	(15,0)	(13,3)	(1,14)	(0,0)	(0,15)	(0,16)	(4,12)	(0,0)	(13,1)	(14,3)	(11,2)
	Taipei	(0,0)	(0,5)	(0,8)	(1,3)	(0,0)	(0,3)	(0,8)	(0,4)	(0,0)	(6,0)	(8,0)	(3,0)
Hangzhou	Beijing	(0,0)	(8,0)	(8,1)	(1,9)	(0,0)	(0,8)	(0,8)	(4,6)	(0,0)	(8,0)	(1,8)	(0,10)
	Qingdao	(0,0)	(5,0)	(0,1)	(1,2)	(0,0)	(0,4)	(0,1)	(0,4)	(0,0)	(1,4)	(0,1)	(2,1)
	Shanghai	(0,0)	(0,0)	(0,0)	(0,0)	(0,0)	(0,0)	(0,0)	(0,0)	(0,0)	(0,0)	(0,0)	(0,0)
	Guangzhou	(2,0)	(7,0)	(9,1)	(1,8)	(0,2)	(0,8)	(0,9)	(2,7)	(1,1)	(5,3)	(9,1)	(8,0)
	Taipei	(0,0)	(0,1)	(0,1)	(1,0)	(0,0)	(0,2)	(0,0)	(1,1)	(0,0)	(2,0)	(0,0)	(1,0)

Continued

Start point	End point	August 9th				August 10th				August 11th			
		[0,6)	[6,12)	[12,18)	[18,24)	[0,6)	[6,12)	[12,18)	[18,24)	[0,6)	[6,12)	[12,18)	[18,24)
Guangzhou	Beijing	(0,0)	(8,0)	(9,0)	(8,3)	(0,0)	(7,1)	(11,2)	(11,0)	(0,0)	(8,0)	(13,0)	(10,1)
	Qingdao	(0,0)	(1,4)	(5,0)	(2,0)	(0,0)	(4,0)	(4,1)	(2,1)	(0,0)	(0,4)	(2,3)	(2,1)
	Shanghai	(1,1)	(17,0)	(6,11)	(0,10)	(0,2)	(0,17)	(2,15)	(5,7)	(4,1)	(13,9)	(16,1)	(9,1)
	Hangzhou	(2,0)	(9,0)	(3,5)	(0,9)	(0,2)	(0,9)	(1,8)	(6,4)	(1,1)	(6,4)	(8,0)	(8,0)
	Taipei	(0,0)	(0,1)	(2,1)	(0,0)	(0,0)	(1,0)	(2,0)	(1,0)	(0,0)	(1,0)	(2,0)	(0,0)
Taipei	Beijing	(0,0)	(1,0)	(1,2)	(1,0)	(0,0)	(1,0)	(2,0)	(2,0)	(0,0)	(0,0)	(3,0)	(2,0)
	Qingdao	(0,0)	(0,1)	(0,2)	(0,0)	(0,0)	(1,0)	(0,0)	(0,0)	(0,0)	(1,0)	(0,0)	(0,0)
	Shanghai	(0,0)	(0,4)	(1,11)	(0,0)	(0,0)	(0,2)	(0,2)	(0,1)	(0,0)	(6,0)	(12,0)	(1,0)
	Hangzhou	(0,0)	(0,0)	(1,1)	(0,1)	(0,0)	(0,1)	(0,1)	(1,1)	(0,0)	(1,0)	(2,0)	(0,0)
	Guangzhou	(0,0)	(0,1)	(3,1)	(0,0)	(0,0)	(0,0)	(3,0)	(1,0)	(0,0)	(1,0)	(2,0)	(0,0)

3. Deep multimodal fusion and multitasking trajectory prediction model

Using deep learning technology, a deep multimodal fusion and multitasking trajectory prediction model is proposed to predict the position of the typhoon [30]. An airport within the predicted position threshold can be regarded as an affected airport, and all takeoffs and landing flights of that airport will be affected. Then, the flights at the airport should take corresponding evasive measures. The core part of this method is trajectory prediction. The more accurate the trajectory prediction is, the more favourable it is for flight scheduling, and the more favourable it is for the optimization of flight scheduling.

3.1 Typhoon trajectory forecast

In this paper, a trajectory prediction model is proposed based on deep multimodal fusion and multitask generation, as shown in Fig. 1. It mainly includes two modules: a deep multimodal fusion module that is formed by deep fusion of the features output by multiple submodal fusion modules and a multitask generation module that uses longitude and latitude as two related tasks for simultaneous prediction. When multiple modalities coexist, we can extract features from multiple modalities at the same time to supplement each other's information. At the same time, we can also capture the dynamic changes of the trajectory in time and space to improve the accuracy of the prediction.

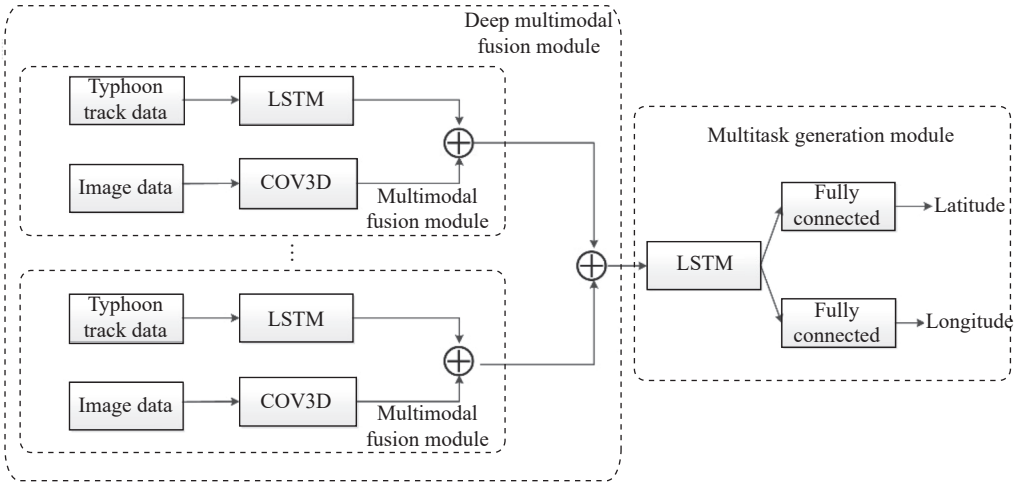

Fig. 1 Deep multimodal fusion and multitask generation trajectory prediction model

(i) Trajectory data training

Trajectory data are common sequence data, and we use long short-term memory (LSTM) to process trajectory data [31]. It can effectively extract the characteristics of changes in time series over time, so we apply LSTM to extract the characteristics of changes in typhoon trajectory over time.

The gates of LSTM at each sequence index position generally include forget gates, input gates and output gates [32]. The forget gate, as the name implies, controls

whether to forget the hidden cell state of the upper layer with a certain probability, as in

$$\boldsymbol{f}^t = \sigma(\boldsymbol{W}_f \cdot [\boldsymbol{h}_{\text{tra}}^{t-1}, \boldsymbol{x}_{\text{tra}}^t] + \boldsymbol{b}_f). \tag{1}$$

Among them, the value of $\boldsymbol{f}^t$ in each dimension is in the range of (0,1), then the information on the dimension whose value is close to 0 will be forgotten, and the information on the dimension whose value is close to 1 will be retained; $\boldsymbol{W}_f$ represents the weight matrix, $\boldsymbol{b}_f$ represents the bias term, and these two parameters are continuously trained by the neural network through training historical data. $\boldsymbol{h}_{\text{tra}}^{t-1}$ is the output of the hidden layer at moment $t-1$ and $\boldsymbol{x}_{\text{tra}}^t$ is the input of the hidden layer at moment t. "·" represents matrix multiplication, and σ represents the sigmoid function.

The input gate is responsible for processing the input of the current sequence position and selectively storing new information in the cell [33]. There are two steps in the input gate. Equation (2) determines the value to be updated and expressed by probability $\boldsymbol{i}^t$. In (3), the function generates a new candidate vector $\tilde{\boldsymbol{C}}^t$ and adds it to the cell state. The two parts combine to form the input gate.

$$\boldsymbol{i}^t = \sigma(\boldsymbol{W}_i \cdot [\boldsymbol{h}_{\text{tra}}^{t-1}, \boldsymbol{x}_{\text{tra}}^t] + \boldsymbol{b}_i), \tag{2}$$

$$\tilde{\boldsymbol{C}}^t = \tanh(\boldsymbol{W}_C \cdot [\boldsymbol{h}_{\text{tra}}^{t-1}, \boldsymbol{x}_{\text{tra}}^t] + \boldsymbol{b}_C), \tag{3}$$

where $\boldsymbol{W}_i$, $\boldsymbol{W}_C$ represents the weight matrix and $\boldsymbol{b}_i$, $\boldsymbol{b}_C$ represents the bias term. The $\tanh(\cdot)$ function is a hyperbolic tangent function.

Before the output gate, the cell state needs to be updated, as shown in (4), and the results of the previous forget gate and input gate will affect the cell state [34]. Here, $*$ represents the Hadamard product.

$$\boldsymbol{C}^t = \boldsymbol{f}^t * \boldsymbol{C}^{t-1} + \boldsymbol{i}^t * \tilde{\boldsymbol{C}}^t \tag{4}$$

The output gate determines what to output, and the output will be based on the LSTM cell state, but it is also a filtered result [35]. As shown in (5) and (6), $\boldsymbol{o}^t$ controls how much the current output $\boldsymbol{C}^t$ can be used, and the value of $\boldsymbol{o}^t$ is between (0, 1). In addition, $\boldsymbol{h}_{\text{tra}}^t$ is the output of the hidden layer at moment t.

$$\boldsymbol{o}^t = \sigma(\boldsymbol{W}_o[\boldsymbol{h}_{\text{tra}}^{t-1}, \boldsymbol{x}_{\text{tra}}^t] + \boldsymbol{b}_o), \tag{5}$$

$$\boldsymbol{h}_{\text{tra}}^t = \boldsymbol{o}^t * \tanh(\boldsymbol{C}^t), \tag{6}$$

where $\boldsymbol{W}_o$ represents the weight matrix and $\boldsymbol{b}_o$ represents the bias term. These two parameters are continuously trained by the neural network through historical training data.

To enable feature fusion of data of multiple modalities, we output a one-dimensional feature in the last LSTM layer; $\boldsymbol{h}_{\text{tra}}^t$ is the final output feature of the trajectory data training part, that is, $\boldsymbol{h}_{\text{tra}}^t \in \mathbf{R}^{\text{dt}}$, and dt is the size of the feature extracted from the trajectory path data.

(ii) Satellite image convolution

LSTM's feature extraction of trajectory data extracts only the change features of the trajectory in time, while the three-dimensional (3D) convolutional neural network (3D CNN) [36] can extract the change characteristics of the trajectory from time and space. In addition, 3D CNNs are more suitable for learning spatiotemporal features than two-dimensional (2D) CNNs, and they can better model temporal and space information through 3D convolution and 3D pooling operations. In a 3D CNN, convolution and pooling operations are performed in space and time, while in a 2D CNN, they are completed only in space. In actual applications, the number and structure of neural networks should be adjusted accordingly based on different application scenarios.

Traditional 2D convolutional neural networks cannot process or need to be combined with other networks to capture the actions of consecutive frames in video data, so this research uses a 3D CNN to process the temporal dimension information of adjacent frames. The satellite image information at each moment is regarded as the m frame, the image data $\boldsymbol{V}_{\text{Ig}}$ are formatted as in (7), and the trajectory changes in time and space are learned through the 3D CNN. Here the abbreviation Ig means image.

$$\boldsymbol{V}_{\text{Ig}} = \text{reshape}\left(\boldsymbol{X}_{\text{Ig}}^1, \boldsymbol{X}_{\text{Ig}}^2, \cdots, \boldsymbol{X}_{\text{Ig}}^m\right) \in \mathbf{R}^{m \times H \times W \times R} \tag{7}$$

where m represents the number of pictures, and $\boldsymbol{X}_{\text{Ig}}^m$ represent the height, width and colour channel of each satellite picture. H, W, R represent the size of the convolution kernel respectively.

The basic principle of 3D convolution is shown in Fig. 2 [37,38]. Each layer of the 3D convolution layer performs a convolution operation on the 3D feature data (or original data) output by the previous layer through the 3D convolution kernel to obtain 3D feature data as the input of the next layer. Assume that i represents the ith 3D convolutional layer, v_{ij} represents the jth 3D feature data output by the ith 3D convolutional layer, H_i, W_i, R_i represent the size of the convolution kernel, and N_i is the number of convolution kernels in the ith convolutional layer.

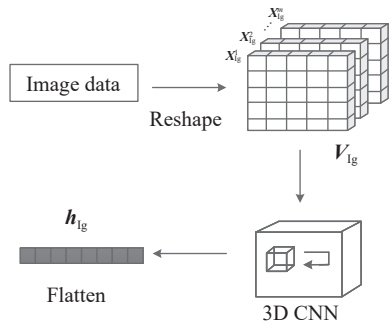

Fig. 2 Basic principle diagram of 3D convolution

Then, the feature value v_{ij} at the position (x,y,z), that is, the 3D convolution process, is as in

$$v_{ij}^{x,y,z} = \mathrm{ReLU}\left(b_{ij} + \sum_{n=0}^{N_i-1}\sum_{h=0}^{H_i-1}\sum_{w=0}^{W_i-1}\sum_{r=0}^{R_i-1}\omega_{ijn}^{hwr} v_{(i-1)n}^{(x+h)(y+w)(z+r)}\right) \quad (8)$$

where ReLU represents the activation function, b_{ij} represents the bias function of the jth 3D feature data of the ith convolutional layer, and ω_{ijn}^{hwr} represents the weight.

The output of 3D convolution is multidimensional feature data. To integrate the features of multiple modalities, we finally use the Flatten layer operation to flatten the result of the 3D convolution, that is, to make the multidimensional feature data one-dimensional, as in

$$\boldsymbol{h}_{\mathrm{Ig}} = \mathrm{Flatten}(\boldsymbol{v}_{\mathrm{Ig}}) \in \mathbf{R}^{\mathrm{di}} \quad (9)$$

where di represents the size of the 3D convolution feature.

(iii) Deep feature fusion

Multimodal fusion of various submodules performs feature fusion between the features $\boldsymbol{h}_{\mathrm{tra}}$ of the training output of the trajectory data and the features $\boldsymbol{h}_{\mathrm{Ig}}$ generated by the convolution of the satellite image [39]. Splicing in the feature dimension forms a new feature $\boldsymbol{H}_{\mathrm{fusion}}$, as shown in

$$\boldsymbol{H}_{\mathrm{fusion}} = \boldsymbol{h}_{\mathrm{tra}} \oplus \boldsymbol{h}_{\mathrm{Ig}} \in \mathbf{R}^{\mathrm{dt+di}} \quad (10)$$

where dt+di represents the size of the feature generated by the multimodal feature fusion module.

A section of multimodal trajectory $\mathrm{Trj} = \{\boldsymbol{X}^1, \boldsymbol{X}^2, \cdots, \boldsymbol{X}^N\}$ (its length N) is divided into k multimodal subtrajectories $\mathrm{subTrj}_1 = \{\boldsymbol{X}^1, \boldsymbol{X}^2, \cdots, \boldsymbol{X}^m\}, \mathrm{subTrj}_2 = \{\boldsymbol{X}^{1+2\tau}, \boldsymbol{X}^{2+2\tau}, \cdots, \boldsymbol{X}^{m+2\tau}\}, \cdots, \mathrm{subTrj}_k = \{\boldsymbol{X}^{1+k\tau}, \boldsymbol{X}^{2+k\tau}, \cdots, \boldsymbol{X}^{m+k\tau}\}$ (each length m) through a sliding window, where τ is the sliding step length, $1 \leqslant m + k\tau \leqslant N$. The reason for dividing the multimodal trajectory is to allow the changes in time and space of the trajectory to be reflected in the characteristics.

The features output by the k multimodal fusion modules are spliced according to the time dimension to form a deep mixed feature, as shown in

$$\boldsymbol{H}_{\mathrm{df}} = \boldsymbol{H}_{\mathrm{fusion}}^1 \oplus \boldsymbol{H}_{\mathrm{fusion}}^2 \oplus \cdots \oplus \boldsymbol{H}_{\mathrm{fusion}}^k \in \mathbf{R}^{k \times df} \quad (11)$$

where $\mathrm{df} = \mathrm{dt} + \mathrm{di}$, and the dimension of the deep fusion feature $\boldsymbol{H}_{\mathrm{df}}$ output by the deep multimodal fusion module is $k \times \mathrm{df}$.

(iv) Multi-task generation module

The deep fusion feature $\boldsymbol{H}_{\mathrm{df}}$ output by the deep multimodal fusion module can be regarded as a time-related series feature data. This module adopts LSTM training deep fusion features and simultaneously predicts the longitude and latitude as related tasks. The prediction results of the longitude and latitude are shown in (12) and (13), respectively. The location information of the trajectory is jointly represented by the longitude and latitude, which are related learning tasks. Therefore, multitask learning can promote the learning effect of longitude and latitude to improve the prediction accuracy.

$$\hat{\boldsymbol{X}}_{\mathrm{longitude}} = \boldsymbol{H}_{\mathrm{df}} \cdot \boldsymbol{W}_{\mathrm{LSTM}} \cdot \boldsymbol{W}_{\mathrm{flon}}, \quad (12)$$

$$\hat{\boldsymbol{X}}_{\mathrm{latitude}} = \boldsymbol{H}_{\mathrm{df}} \cdot \boldsymbol{W}_{\mathrm{LSTM}} \cdot \boldsymbol{W}_{\mathrm{flat}}, \quad (13)$$

where $\boldsymbol{W}_{\mathrm{LSTM}}$ is the weight of the LSTM network training, which is shared in the multitask generation module. $\boldsymbol{W}_{\mathrm{flon}}, \boldsymbol{W}_{\mathrm{flat}}$ represent the weights of the longitude and latitude full-connection layer training, respectively.

3.2 Flight scheduling optimization

By accurately predicting the location of the typhoon's trajectory, necessary measures can be taken to optimize flight scheduling according to the airports within the typhoon's trajectory. Therefore, it is possible to avoid the waste of resources caused by blindly cancelling flights and to avoid flight hazards caused by untimely cancellation of flights [40]. According to the convenience query website (https://airportcode.bmcx.com/CAN_428__ac/), the location information of major airports collected is shown in Table 3. To check the accuracy of this information, we compare it with Baidu Map information. Take Beijing Capital Airport as an example, the coordinate information displayed on Baidu Map is (40.08 N,116.60 E), and the information provided by the website is (40.08 N, 116.58 E). It can be found that the coordinates of the airport displayed on Baidu Map are almost consistent with the information provided by the website. After all, the location information provided by different tools is never exactly the same. Data can be considered usable as long as it is within a reasonable margin of error for this research.

Table 3 Airport location information

Airport	Location
Beijing Capital Airport	(40.08 N, 116.58 E)
Beijing Daxing Airport	(39.51 N, 116.41 E)
Qingdao Liuting Airport	(36.27 N, 120.38 E)
Shanghai Hongqiao Airport	(31.19 N, 121.34 E)
Shanghai Pudong Airport	(31.14 N, 121.79 E)
Hangzhou Xiaoshan Airport	(30.33 N, 120.22 E)
Guangzhou Baiyun Airport	(23.18 N, 113.26 E)
Taipei Taoyuan Airport	(25.09 N, 121.60 E)
Taipei Songshan Airport	(25.06 N, 121.55 E)

According to the published data of the Tropical Cyclone Data Center of the China Meteorological Administration (http://tcdata.typhoon.org), the real coordinate information of Lichma at 0:00, 6:00, 12:00, and 18:00 from August 9th to August 11th are summarized in Table 4. Assuming that the distance L between the airport and Lichma is within the threshold τ, as in (14), it is

determined that the airport will be affected and the flight at this airport should be cancelled. In this case, Beijing, Shanghai and Taipei have two airports, so as long as one airport in the area is affected and the flights are cancelled, the flights at the other airport would also be cancelled.

$$L = (x_{\text{typhoon}} - x_{\text{airport}})^2 - (y_{\text{typhoon}} - y_{\text{airport}}\sqrt{})^2 \leqslant \tau \quad (14)$$

Table 4 Location information of Lichma at 0:00, 6:00, 12:00, and 18:00 from August 9th to August 11th

Date	Time	Location
August 9th	0:00	(26.5 N, 123.4 E)
	6:00	(27.0 N, 122.5 E)
	12:00	(27.5 N, 122.0 E)
	18:00	(28.3 N, 121.4 E)
August 10th	0:00	(28.9 N, 120.8 E)
	6:00	(29.9 N, 120.3 E)
	12:00	(30.7 N, 120.2 E)
	18:00	(31.7 N, 120.5 E)
August 11th	0:00	(33.6 N, 120.2 E)
	6:00	(34.8 N, 119.9 E)
	12:00	(35.8 N, 120.2 E)
	18:00	(36.9 N, 119.7 E)

4. Results

In this section, we will provide numerical tests on a real case of flight cancellations affected by typhoons for the proposed deep multimodal fusion and multitasking trajectory prediction model.

4.1 Flight scheduling under real typhoon data

Under the real typhoon trajectory, when $\tau = 1.5°$ is taken, the affected regional flights are shown in Table 5. The red colour in the table indicates that flights from the departure place to the destination are prohibited from taking off at that time. It shows which flights will be affected and which flights will not be affected when the typhoon track is known. From 0:00-6:00 on August 10th, Hangzhou and Shanghai flights will be affected; from 6:00-12:00 on August 10th, Hangzhou flights will be affected; from 12:00-18: 00 on August 10th, Hangzhou flights will be affected; from 18:00-24:00 on August 10th, Hangzhou and Shanghai flights will be affected; from 12:00-18:00 on August 11th, Qingdao flights will be affected; and from 18:00-24:00 on August 11th, Qingdao flights will be affected.

Table 5 Influences of the actual location of typhoon Lichma on the arrival and cancellation of flights in Beijing, Qingdao, Shanghai, Hangzhou, Guangzhou and Taipei from August 9th to August 11th

Start point	End point	August 9th				August 10th				August 11th			
		[0,6)	[6,12)	[12,18)	[18,24)	[0,6)	[6,12)	[12,18)	[18,24)	[0,6)	[6,12)	[12,18)	[18,24)
Beijing	Qingdao	(0,0)	(6,0)	(2,0)	(2,2)	(0,0)	(6,0)	(1,1)	(4,2)	(0,0)	(2,7)	(0,2)	(0,8)
	Shanghai	(0,0)	(17,1)	(3,15)	(0,14)	(0,0)	(0,18)	(1,22)	(0,13)	(0,0)	(17,3)	(18,2)	(11,3)
	Hangzhou	(1,0)	(11,0)	(2,4)	(0,8)	(0,1)	(2,9)	(1,7)	(4,4)	(1,0)	(11,1)	(5,1)	(9,0)
	Guangzhou	(0,0)	(13,0)	(13,1)	(4,3)	(0,0)	(9,4)	(13,0)	(7,0)	(0,0)	(12,1)	(13,0)	(7,0)
	Taipei	(0,0)	(2,2)	(1,0)	(1,0)	(0,0)	(2,0)	(2,0)	(1,0)	(0,0)	(2,0)	(1,0)	(2,0)
Qingdao	Beijing	(0,0)	(4,0)	(4,1)	(2,1)	(0,0)	(4,0)	(5,0)	(3,1)	(0,0)	(2,2)	(1,7)	(0,5)
	Shanghai	(0,0)	(8,1)	(6,3)	(0,10)	(0,0)	(0,11)	(0,9)	(0,9)	(0,0)	(6,5)	(2,7)	(2,7)
	Hangzhou	(0,0)	(3,0)	(3,1)	(0,1)	(0,0)	(0,4)	(0,4)	(0,2)	(0,0)	(2,1)	(1,3)	(0,1)
	Guangzhou	(0,0)	(3,0)	(4,0)	(4,0)	(0,0)	(3,0)	(4,0)	(3,2)	(0,0)	(3,0)	(1,3)	(0,5)
	Taipei	(0,0)	(0,1)	(0,2)	(0,0)	(0,0)	(0,0)	(1,0)	(0,0)	(0,0)	(0,0)	(1,0)	(0,0)
Shanghai	Beijing	(0,0)	(18,0)	(13,4)	(1,14)	(0,0)	(1,16)	(0,19)	(0,15)	(0,0)	(8,8)	(13,4)	(14,1)
	Qingdao	(0,0)	(9,2)	(7,1)	(0,11)	(0,0)	(0,11)	(0,8)	(0,10)	(0,0)	(0,12)	(3,4)	(3,7)
	Hangzhou	(0,0)	(0,0)	(0,0)	(0,0)	(0,0)	(0,0)	(0,0)	(0,0)	(0,0)	(0,0)	(0,0)	(0,0)
	Guangzhou	(0,0)	(15,0)	(13,3)	(1,14)	(0,0)	(0,15)	(0,16)	(4,12)	(0,0)	(13,1)	(14,3)	(11,2)
	Taipei	(0,0)	(0,5)	(0,8)	(1,3)	(0,0)	(0,3)	(0,8)	(0,4)	(0,0)	(6,0)	(8,0)	(3,0)
Hangzhou	Beijing	(0,0)	(8,0)	(8,1)	(1,9)	(0,0)	(0,8)	(0,8)	(4,6)	(0,0)	(8,0)	(1,8)	(0,10)
	Qingdao	(0,0)	(5,0)	(0,1)	(1,2)	(0,0)	(0,4)	(0,1)	(0,4)	(0,0)	(1,4)	(0,1)	(2,1)
	Shanghai	(0,0)	(0,0)	(0,0)	(0,0)	(0,0)	(0,0)	(0,0)	(0,0)	(0,0)	(0,0)	(0,0)	(0,0)
	Guangzhou	(2,0)	(7,0)	(9,1)	(1,8)	(0,2)	(0,8)	(0,9)	(2,7)	(1,1)	(5,3)	(9,1)	(8,0)
	Taipei	(0,0)	(0,1)	(0,1)	(1,0)	(0,0)	(0,2)	(0,0)	(1,1)	(0,0)	(2,0)	(0,0)	(1,0)

Continued

Start point	End point	August 9th				August 10th				August 11th			
		[0,6)	[6,12)	[12,18)	[18,24)	[0,6)	[6,12)	[12,18)	[18,24)	[0,6)	[6,12)	[12,18)	[18,24)
Guangzhou	Beijing	(0,0)	(8,0)	(9,0)	(8,3)	(0,0)	(7,1)	(11,2)	(11,0)	(0,0)	(8,0)	(13,0)	(10,1)
	Qingdao	(0,0)	(1,4)	(5,0)	(2,0)	(0,0)	(4,0)	(4,1)	(2,1)	(0,0)	(0,4)	(2,3)	(2,1)
	Shanghai	(1,1)	(17,0)	(6,11)	(0,10)	(0,2)	(0,17)	(2,15)	(5,7)	(4,1)	(13,9)	(16,1)	(9,1)
	Hangzhou	(2,0)	(9,0)	(3,5)	(0,9)	(0,2)	(0,9)	(1,8)	(6,4)	(1,1)	(6,4)	(8,0)	(8,0)
	Taipei	(0,0)	(0,1)	(2,1)	(0,0)	(0,0)	(1,0)	(2,0)	(1,0)	(0,0)	(1,0)	(2,0)	(0,0)
Taipei	Beijing	(0,0)	(1,0)	(1,2)	(1,0)	(0,0)	(1,0)	(2,0)	(2,0)	(0,0)	(0,0)	(3,0)	(2,0)
	Qingdao	(0,0)	(0,1)	(0,2)	(0,0)	(0,0)	(1,0)	(0,0)	(0,0)	(0,0)	(1,0)	(0,0)	(0,0)
	Shanghai	(0,0)	(0,4)	(1,11)	(0,0)	(0,0)	(0,2)	(0,2)	(0,1)	(0,0)	(6,0)	(12,0)	(1,0)
	Hangzhou	(0,0)	(0,0)	(1,1)	(0,1)	(0,0)	(0,1)	(0,1)	(1,1)	(0,0)	(1,0)	(2,0)	(0,0)
	Guangzhou	(0,0)	(0,1)	(3,1)	(0,0)	(0,0)	(0,0)	(3,0)	(1,0)	(0,0)	(1,0)	(2,0)	(0,0)

A comparison between Table 5 and Table 2 shows that in fact, many flights do not need to be cancelled, but airlines have actually cancelled them. For example, all airports would not be affected during August 9th, but from Table 2, it can be seen that some flights on August 9 were cancelled, which caused a waste of resources. From 12:00 to 18:00 on August 11th, Qingdao Liuting Airport will be affected, but according to the information shown in Table 2, there are still flights arriving at Qingdao Liuting Airport or departing from Qingdao Liuting Airport, which is very dangerous.

4.2 Flight scheduling under forecast typhoon data

If the location of the typhoon can be predicted more accurately, the waste of resources can be avoided as much as possible, and the risk of air crashes can also be reduced. Using the deep multimodal fusion and multitasking trajectory prediction model shown in Fig. 1, it is predicted that, from August 9th to August 11th, the trajectory coordinates of Lichma at 0:00, 6:00, 12:00, and 18:00 are as shown in Table 6.

Because the predicted trajectory would have a certain deviation relative to the real trajectory, we set the threshold τ value to be larger than the real typhoon trajectory. When τ is set to 2.0°, the affected regional flights are shown in Table 7. It shows which flights would be affected within the threshold range and which flights would not be affected by predicting the typhoon trajectory. From 0:00-6:00 on August 10th, Hangzhou and Shanghai flights would be affected; from 6:00-12:00 on August 10th, Hangzhou flights would be affected; from 12:00-18:00 on August 10th, Hangzhou flights would be affected; from 18:00-24:00 on August 10th, Hangzhou and Shanghai flights would be affected; from 0:00-6:00 on August 11th, Hangzhou and Shanghai flights would be affected; from 12:00-18:00 on August 11th, Qingdao flights would be affected; and from 18:00 to 24:00 on August 11th, Qingdao flights would be affected.

Table 6 Predicted trajectory location of Lichma at 0:00, 6:00, 12:00, and 18:00 from August 9th to August 11th

Date	Time	Predicted trajectory location
August 9th	0:00	(26.658 N, 124.986 E)
	6:00	(27.007 N, 123.023 E)
	12:00	(27.905 N, 121.832 E)
	18:00	(28.424 N, 121.794 E)
August 10th	0:00	(29.593 N, 121.144 E)
	6:00	(28.627 N, 119.829 E)
	12:00	(30.038 N, 1196.68 E)
	18:00	(307.72 N, 120.367 E)
August 11th	0:00	(321.87 N, 120.733 E)
	6:00	(34.672 N, 120.636 E)
	12:00	(35.968 N, 119.747 E)
	18:00	(374.26 N, 119.390 E)

Table 7 Influences of the predicted location of Typhoon Lichma on the arrival and cancellation of flights in Beijing, Qingdao, Shanghai, Hangzhou, Guangzhou and Taipei from August 9th to August 11th

Start point	End point	August 9th				August 10th				August 11th			
		[0,6)	[6,12)	[12,18)	[18,24)	[0,6)	[6,12)	[12,18)	[18,24)	[0,6)	[6,12)	[12,18)	[18,24)
Beijing	Qingdao	(0,0)	(6,0)	(2,0)	(2,2)	(0,0)	(6,0)	(1,1)	(4,2)	(0,0)	(2,7)	(0,2)	(0,8)
	Shanghai	(0,0)	(17,1)	(3,15)	(0,14)	(0,0)	(0,18)	(1,22)	(0,13)	(0,0)	(17,3)	(18,2)	(11,3)

Continued

Start point	End point	August 9th				August 10th				August 11th			
		[0,6)	[6,12)	[12,18)	[18,24)	[0,6)	[6,12)	[12,18)	[18,24)	[0,6)	[6,12)	[12,18)	[18,24)
Beijing	Hangzhou	(1,0)	(11,0)	(2,4)	(0,8)	(0,1)	(2,9)	(1,7)	(4,4)	(1,0)	(11,1)	(5,1)	(9,0)
	Guangzhou	(0,0)	(13,0)	(13,1)	(4,3)	(0,0)	(9,4)	(13,0)	(7,0)	(0,0)	(12,1)	(13,0)	(7,0)
	Taipei	(0,0)	(2,2)	(1,0)	(1,0)	(0,0)	(2,0)	(2,0)	(1,0)	(0,0)	(2,0)	(1,0)	(2,0)
Qingdao	Beijing	(0,0)	(4,0)	(4,1)	(2,1)	(0,0)	(4,0)	(5,0)	(3,1)	(0,0)	(2,2)	(1,7)	(0,5)
	Shanghai	(0,0)	(8,1)	(6,3)	(0,10)	(0,0)	(0,11)	(0,9)	(0,9)	(0,0)	(6,5)	(2,7)	(2,7)
	Hangzhou	(0,0)	(3,0)	(3,1)	(0,1)	(0,0)	(0,4)	(0,4)	(0,2)	(0,0)	(2,1)	(1,3)	(0,1)
	Guangzhou	(0,0)	(3,0)	(4,0)	(4,0)	(0,0)	(3,0)	(4,0)	(3,2)	(0,0)	(3,0)	(1,3)	(0,5)
	Taipei	(0,0)	(0,1)	(0,2)	(0,0)	(0,0)	(0,0)	(1,0)	(0,0)	(0,0)	(0,0)	(1,0)	(0,0)
Shanghai	Beijing	(0,0)	(18,0)	(13,4)	(1,14)	(0,0)	(1,16)	(0,19)	(0,15)	(0,0)	(8,8)	(13,4)	(14,1)
	Qingdao	(0,0)	(9,2)	(7,1)	(0,11)	(0,0)	(0,11)	(0,8)	(0,10)	(0,0)	(0,12)	(3,4)	(3,7)
	Hangzhou	(0,0)	(0,0)	(0,0)	(0,0)	(0,0)	(0,0)	(0,0)	(0,0)	(0,0)	(0,0)	(0,0)	(0,0)
	Guangzhou	(0,0)	(15,0)	(13,3)	(1,14)	(0,0)	(0,15)	(0,16)	(4,12)	(0,0)	(13,1)	(14,3)	(11,2)
	Taipei	(0,0)	(0,5)	(0,8)	(1,3)	(0,0)	(0,3)	(0,8)	(0,4)	(0,0)	(6,0)	(8,0)	(3,0)
Hangzhou	Beijing	(0,0)	(8,0)	(8,1)	(1,9)	(0,0)	(0,8)	(0,8)	(4,6)	(0,0)	(8,0)	(1,8)	(0,10)
	Qingdao	(0,0)	(5,0)	(0,1)	(1,2)	(0,0)	(0,4)	(0,1)	(0,4)	(0,0)	(1,4)	(0,1)	(2,1)
	Shanghai	(0,0)	(0,0)	(0,0)	(0,0)	(0,0)	(0,0)	(0,0)	(0,0)	(0,0)	(0,0)	(0,0)	(0,0)
	Guangzhou	(2,0)	(7,0)	(9,1)	(1,8)	(0,2)	(0,8)	(0,9)	(2,7)	(1,1)	(5,3)	(9,1)	(8,0)
	Taipei	(0,0)	(0,1)	(0,1)	(1,0)	(0,0)	(0,2)	(0,0)	(1,1)	(0,0)	(2,0)	(0,0)	(1,0)
Guangzhou	Beijing	(0,0)	(8,0)	(9,0)	(8,3)	(0,0)	(7,1)	(11,2)	(11,0)	(0,0)	(8,0)	(13,0)	(10,1)
	Qingdao	(0,0)	(1,4)	(5,0)	(2,0)	(0,0)	(4,0)	(4,1)	(2,1)	(0,0)	(0,4)	(2,3)	(2,1)
	Shanghai	(1,1)	(17,0)	(6,11)	(0,10)	(0,2)	(0,17)	(2,15)	(5,7)	(4,1)	(13,9)	(16,1)	(9,1)
	Hangzhou	(2,0)	(9,0)	(3,5)	(0,9)	(0,2)	(0,9)	(1,8)	(6,4)	(1,1)	(6,4)	(8,0)	(8,0)
	Taipei	(0,0)	(0,1)	(2,1)	(0,0)	(0,0)	(1,0)	(2,0)	(1,0)	(0,0)	(1,0)	(2,0)	(0,0)
Taipei	Beijing	(0,0)	(1,0)	(1,2)	(1,0)	(0,0)	(1,0)	(2,0)	(2,0)	(0,0)	(0,0)	(3,0)	(2,0)
	Qingdao	(0,0)	(0,1)	(0,2)	(0,0)	(0,0)	(1,0)	(0,0)	(0,0)	(0,0)	(1,0)	(0,0)	(0,0)
	Shanghai	(0,0)	(0,4)	(1,11)	(0,0)	(0,0)	(0,2)	(0,2)	(0,1)	(0,0)	(6,0)	(12,0)	(1,0)
	Hangzhou	(0,0)	(0,0)	(1,1)	(0,1)	(0,0)	(0,1)	(0,1)	(1,1)	(0,0)	(1,0)	(2,0)	(0,0)
	Guangzhou	(0,0)	(0,1)	(3,1)	(0,0)	(0,0)	(0,0)	(3,0)	(1,0)	(0,0)	(1,0)	(2,0)	(0,0)

By comparing Table 7 with Table 2, according to the predicted results, all flights on August 9th would not be affected; Qingdao Liuting Airport would be affected from 12:00 to 18:00 on August 11th. Comparing Table 7 with Table 5, although the predicted results cannot optimize flight scheduling as much as the real typhoon trajectory, compared with Table 2, flight optimization can still be carried out to a greater extent.

4.3 Comparison of flight passability rate

We use η_{ban} to denote the number of time periods during which a flight is cancelled, and η_{total} denotes the number of all time periods, as shown in (15) to express the flight passability rate, that is, the proportion of the time periods during which the flight is safe to fly in all time periods.

$$\eta = 1 - \frac{\eta_{\text{ban}}}{\eta_{\text{total}}} \tag{15}$$

In Table 2, when we calculate the flight passability rate, if there are flight cancellations within the time period, it is counted in η_{ban}. The flight passability rate shown in Table 2 could be calculated as $\eta = 1 - \frac{156}{320} = 0.512\,5$. The flight passability rate shown in Table 5 is $\eta = 1 - \frac{62}{320} \approx 0.806$. The flight passability rate shown in Table 7 is $\eta = 1 - \frac{86}{320} \approx 0.731$.

Therefore, under the condition of a known typhoon trajectory, the flight passability rate is the highest, namely, the flight scheduling is the best and the resource utilization rate is the highest. Although the flight passability rate under the forecast result is lower than the known conditions of the typhoon, compared with the real flight

schedule, the flight passability rate can be greatly improved through prediction, so the precise predicted result can optimize the flight schedule.

5. Conclusions

To contain the negative impacts of extreme weather (typhoon in this research), airlines, airports, associations and regulatory bodies are considered ways to better address fallouts from climate change and extreme weather conditions. They are turning to flight scheduling optimization under typhoon weather for solutions that mitigate some of these challenges. In this research, a deep multimodal fusion and multitasking trajectory prediction model is proposed as an automated planning tool that analyses flight schedules and generates optimal resource levels. Actual case studies have shown that the algorithm converges quickly, which can effectively reduce the number of unnecessary flight cancellations compared to existing flight scheduling and provide help for the new generation of flight scheduling systems to improve the prediction reliability under extreme weather conditions.

Major future research work will include discussing other adverse weather events, e.g., fog, snow storms, and intense falls; and considering more comprehensive uncertainties, e.g., airport capacity, holidays, and epidemic situations. Looking forward to the future development of artificial intelligence technology, further advance measures will be implemented to both predict weather impacts and minimize their disruptions on air transportation and related operations.

References

[1] GUI G, LIU F, SUN J L, et al. Flight delay prediction based on aviation big data and machine learning. IEEE Trans. on Vehicular Technology, 2020, 69(1): 140–150.

[2] WANG H J, SUN J Q, FAN K. Relationships between the North Pacific Oscillation and the typhoon/hurricane frequencies. Science in China, 2007, 50(9): 1409–1416.

[3] KOESDWIADY A, SOUA R, KARRAY F. Improving traffic flow prediction with weather information in connected cars: a deep learning approach. IEEE Trans. on Vehicular Technology, 2016, 65(12): 9508–9517.

[4] ARAB A, TEKIN E, KHODAEI A, et al. System hardening and condition-based maintenance for electric power infrastructure under hurricane effects. IEEE Trans. on Reliability, 2016, 65(3): 1457–1470.

[5] LI Y H, WANG A J, QIAO L, et al. The impact of typhoon Morakot on the modern sedimentary environment of the mud deposition center off the Zhejiang–Fujian coast, China. Continental Shelf Research, 2012, 37: 92−100.

[6] GUO T J, LI G S. Study on methods to identify the impact factors of economic losses due to typhoon storm surge based on confirmatory factor analysis. Natural Hazards, 2020, 100(2): 515–534.

[7] ETANI N. Development of a predictive model for on-time arrival flight of airliner by discovering correlation between flight and weather data. Journal of Big Data, 2019, 6(1): 85–98.

[8] XU Y, DALMAU R, MELGOSA M, et al. A framework for collaborative air traffic flow management minimizing costs for airspace users: enabling trajectory options and flexible pre-tactical delay management. Transportation Research Part B: Methodological, 2020, 134: 229–255.

[9] CAO Y K, ZHU C P, WANG Y J, et al. A method of reducing flight delay by exploring internal mechanism of flight delays. Journal of Advanced Transportation, 2019, 2019: 7069380.

[10] KHAKSAR H, SHEIKHOLESLAMI A. A model for incorporating robustness into flight planning. Proceedings. of the Institution of Civil Engineers-Transport, 2018, 171(5): 275–285.

[11] WEI M, SUN B, WU W, et al. A multiple objective optimization model for aircraft arrival and departure scheduling on multiple runways. Mathematical Biosciences and Engineering, 2020, 17(5): 5545–5560.

[12] TANG F, LIU S, DONG X Y, et al. Aircraft ground service scheduling problems and partheno-genetic algorithm with hybrid heuristic rule. Proc. of the IEEE 7th Annual International Conference on CYBER Technology in Automation, Control, and Intelligent Systems, 2017: 551−555.

[13] CECEN R K, CETEK C, KAYA O. Aircraft sequencing and scheduling in TMAs under wind direction uncertainties. Aeronautical Journal New Series, 2020, 124(1282): 1896–1912.

[14] ABDELGHANY A, ABDELGHANY K, AZADIAN F. Airline flight schedule planning under competition. Computers & Operations Research, 2017, 87: 20−39.

[15] WANG Z J, ZHANG X J. An approach of flight scheduling optimization meet the time conformance monitoring. Proc. of the 13th World Congress on Intelligent Control and Automation, 2018: 1647−1651.

[16] KENAN N, JEBALI A, DIABAT A. An integrated flight scheduling and fleet assignment problem under uncertainty. Computers & Operations Research, 2018, 100: 333–342.

[17] XIAO M M, CAI K Q, ABBASS H A. Hybridized encoding for evolutionary multi-objective optimization of air traffic network flow: a case study on China. Transportation Research, Part E. Logistics and Transportation Review, 2018, 115: 35–55.

[18] SAFAK O, CAVUS O, AKTURK M. Multi-stage airline scheduling problem with stochastic passenger demand and non-cruise times. Transportation Research, Part B: Methodological, 2018, 114: 39−67.

[19] TAKEICHI N. Nominal flight time optimization for arrival time scheduling through estimation/resolution of delay accumulation. Transportation Research, Part C: Emerging technologies, 2017, 77: 433−443.

[20] GU J W, TANG X M, HONG W J, et al. Real-time optimization of short-term flight profiles to control time of arrival. Aerospace Science & Technology, 2019, 84: 1164–1174.

[21] NG K K H, LEE C K M, CHAN F T S, et al. Robust aircraft sequencing and scheduling problem with arrival/departure delay using the min-max regret approach. Transportation Research Part E: Logistics & Transportation Review, 2017, 106: 115–136.

[22] GENG X, HU M H. Simulated annealing method-based flight schedule optimization in multiairport systems. Mathematical Problems in Engineering, 2020, 2020: 4731918.

[23] YANG Y C, GAO Z C, HE C. Stochastic terminal flight

arrival and departure scheduling problem under performance-based navigation environment. Transportation Research Part C: Emerging Technologies, 2020, 119: 102735.
[24] HAN Y X, ZHANG J W, HUANG X Q. Study of the optimization model for traffic flow. Computers & Industrial Engineering, 2019, 136: 429–435.
[25] ZHAO D L, TAN Y J, CHENG R, et al. The optimal aircraft scheduling model based on network model. Proc. of the 36th Chinese Control Conference, 2017: 2935−2940.
[26] HONG Y K, CHOI B H, KIM Y. Two-stage stochastic programming based on particle swarm optimization for aircraft sequencing and scheduling. IEEE Trans. on Intelligent Transportation Systems, 2018, 20(4): 1365–1377.
[27] CHEN X D, YU H, CAO K, et al. Uncertainty-aware flight scheduling for airport throughput and flight delay optimization. IEEE Trans. on Aerospace & Electronic Systems, 2020, 56(2): 853−862.
[28] ZHANG L, HUANG Z Y, LIU W, et al. Weather radar echo prediction method based on convolution neural network and long short-term memory networks for sustainable e-agriculture. Journal of Cleaner Production, 2021, 298: 126776.
[29] FEEYO TECHNOLOGY. Flight status. [2021-01-03]. http://www.variflight.com.
[30] MOHAMED R. Deep multimodal fusion: a hybrid approach. International Journal of Computer Vision, 2018, 126: 440–456.
[31] QIN W T, TANG J, LU C, et al. Trajectory prediction based on long short-term memory network and Kalman filter using hurricanes as an example. Computational Geosciences, 2021, 25: 1005–1023.
[32] GREFF K, SRIVASTAVA R K, KOUTNIK J, et al. LSTM: a search space odyssey. IEEE Trans. on Neural Networks and Learning Systems, 2017, 28(10): 2222–2232.
[33] YU Y, SI X S, HU C H, et al. A review of recurrent neural networks: LSTM cells and network architectures. Neural Computation, 2019, 31(7): 1235–1270
[34] ZHOU X K, HU Y Y, LIANG W, et al. Variational LSTM enhanced anomaly detection for industrial big data. IEEE Trans. on Industrial Informatics, 2021, 17(5): 3469–3477.
[35] YUAN X H, CHEN C, JIANG M, et al. Prediction interval of wind power using parameter optimized Beta distribution based LSTM model. Applied Soft Computing, 2019, 82(2): 105550.
[36] JIN K H, MCCANN M T, FROUSTEY E, et al. Deep convolutional neural network for inverse problems in imaging. IEEE Trans. on Image Processing, 2017, 26(9): 4509–4522.
[37] SARIGUL M, OZYILDIRIM B M. AVC M. Differential convolutional neural network. Neural Networks, 2019, 116: 279–287.
[38] YING X Y, WANG L G, WANG Y Q, et al. Deformable 3D convolution for video super-resolution. IEEE Signal Processing Letters, 2020, 27: 1500–1504.
[39] CHAIB S, LIU H, GU Y F, et al. Deep feature fusion for VHR remote sensing scene classification. IEEE Trans. on Geoscience and Remote Sensing, 2017, 55(8): 4775–4787.
[40] TANG J, LIU G, PAN Q T. A review on representative swarm intelligence algorithms for solving optimization problems: applications and trends. IEEE/CAA Journal of Automatica Sinica, 2021, 8(10): 1627–1643.

Biographies

TANG Jun was born in 1988. He was dedicated to his Ph.D. research in the Technical Innovation Cluster on Aeronautical Management, Autonomous University of Barcelona. He is currently an assistant professor at the Science and Technology on Information Systems Engineering Laboratory, National University of Defense Technology. His research interests include logistic systems, causal modelling, state space, air traffic management, and discrete event simulation.
E-mail: tangjun06@nudt.edu.cn

QIN Wanting was born in 1996. She received her B.S. and M.S. degrees from Shijiazhuang Tiedao University in 2011 and 2015, respectively, and now is working for her Ph.D. degree at the College of Systems Engineering, National University of Defense Technology. Her research interests include trajectory data mining, artificial intelligent, state space and deep learning.
E-mail: qinwt@nudt.edu.cn

PAN Qingtao was born in 1996. He received his B.S. degree from Ocean University of China in 2020. He is currently a Ph.D. student in the Science and Technology on Information Systems Engineering Laboratory, National University of Defense Technology, majoring in control science and engineering. His research interests include intelligent optimization algorithm, system simulation and cluster control.
E-mail: panqingtao@nudt.edu.cn

LAO Songyang was born in 1968. He received his B.S. degree in information system engineering and Ph.D. degree in system engineering from the National University of Defense Technology, Changsha, China, in 1990 and 1996, respectively. He joined National University of Defense Technology as a faculty member, in 1996, where he is currently a professor and the dean of the College of Systems Engineering. He was a visiting scholar with Dublin City University, Irish, from 2004 to 2005. His research interests include image processing, video analysis and human-computer interaction.
E-mail: laosongyang@vip.sina.com